Microstructural characterization of crack-healing enabled by bacteria-embedded polylactic acid (PLA) capsules

He, Shan; Wan, Zhi; Chen, Yu; Jonkers, Henk M.; Schlangen, Erik

DOI
10.1016/j.cemconcomp.2023.105271

Publication date
2023

Document Version
Final published version

Published in
Cement and Concrete Composites

Citation (APA)
He, S., Wan, Z., Chen, Y., Jonkers, H. M., & Schlangen, E. (2023). Microstructural characterization of crack-healing enabled by bacteria-embedded polylactic acid (PLA) capsules. *Cement and Concrete Composites*, *143*, Article 105271. https://doi.org/10.1016/j.cemconcomp.2023.105271

Cement and Concrete Composites 143 (2023) 105271

Contents lists available at ScienceDirect

Cement and Concrete Composites

journal homepage: www.elsevier.com/locate/cemconcomp

Microstructural characterization of crack-healing enabled by bacteria-embedded polylactic acid (PLA) capsules

Shan He *, Zhi Wan, Yu Chen, Henk M. Jonkers, Erik Schlangen

Microlab, Faculty of Civil Engineering and Geosciences, Delft University of Technology, 2628 CN, Delft, the Netherlands

ARTICLE INFO

Keywords:
Self-healing
Bacteria
PLA
SHCC
BSE

ABSTRACT

The current study investigates short-term and long-term crack-healing behaviour of mortars embedded with bacteria-based poly-lactic acid (PLA) capsules under both ideal and realistic environmental conditions. Two sets of specimens were prepared and subjected to different healing regimes, with the first set kept in a mist room for varying short durations (*i.e.*, 1 week, 2 weeks, 3 weeks and 8 weeks) and the second set placed in an unsheltered outdoor environment for a long-term healing process (*i.e.*, 1 year). Alteration of microstructure because of self-healing was characterized by backscattered electron (BSE) imaging and energy dispersive X-ray spectroscopy (EDS) via crack cross-sections. Results show that visible crack healing enabled by bacteria began after 2 weeks in a humid environment. The healing products initially precipitated at crack mouths and gradually moved deeper into cracks, with the precipitated calcium carbonate crystals growing larger over time. After 8 weeks, healing products can be found even a few millimetres deep inside cracks. Observations of crack healing in a realistic environment revealed significant differences compared to healing under controlled conditions. While no healing products can be found at crack mouths, a substantial healing process was observed throughout the entire crack depth. It is likely that the environmental actions such as rainfall and/or freeze and thaw cycles may have worn away the healing products at crack mouths and thus led to a deeper ingress of oxygen into cracks, which promoted the activation of healing agents and associated calcium carbonate precipitation deep inside a crack.

1. Introduction

Micro-cracking is a common occurrence in reinforced concrete structures and can be caused by various factors, including mechanical loading, early-age shrinkage, thermal effects, and freeze-thaw cycles, etc. If micro-cracks form a continuous network or develop into larger cracks, they may substantially decrease the durability of concrete by reducing the resistance of concrete against the ingress of aggressive substances. Nevertheless, not all micro-cracks pose a threat to the integrity of structures. Studies have shown that small cracks in concrete can self-heal under certain conditions, a phenomenon known as "autogenous healing" [1,2]. This healing occurs through a combination of different chemical, physical, and mechanical processes [3,4], with the precipitation of calcium carbonate being the most significant factor.

Although all concrete contains inherent healing capacity, this autogenous healing mechanism is only efficient for small cracks and can hardly be relied upon. To promote the healing performance of concrete, research has been carried out over the last decade either to stimulate the autogenous self-healing capacity (*e.g.*, via the use of mineral additives [2,5], crystalline admixtures [6,7], or superabsorbent polymers [8]), or to develop novel autonomous self-healing mechanisms (*e.g.*, via the application of micro- [9], macro- [10], or vascular-encapsulated polymers [11], minerals, or bacteria [12]). Among all self-healing approaches, the use of encapsulated bacteria as a healing agent has the greatest potential for long-lasting and active crack repair, while at the same time representing the most applicable healing agent to be used in full-scale concrete elements.

Jonkers et al. [12] first introduced a bacteria-based agent, which consists of bacterial spores and an organic mineral precursor compound for providing autonomous healing potential to concrete under aerobic conditions. The bacteria spores activated by crack-induced ingress of water can germinate into active vegetative cells, which then convert mineral precursor to calcium carbonate through aerobic metabolism. The calcium carbonate crystals can then fill the cracks, resulting in the regain of functional properties (*e.g.*, water tightness). Different carriers for encapsulating the bio-agents have been developed, including light-weight aggregate [13], microcapsules [14], bio-granules [15] and polymeric substrates [16,17]. Recently, Mors and Jonkers [17] have

* Corresponding author. Stevinweg 1, 2628 CN, Delft, the Netherlands.
E-mail address: s.he-2@tudelft.nl (S. He).

https://doi.org/10.1016/j.cemconcomp.2023.105271
Received 30 April 2023; Received in revised form 6 August 2023; Accepted 23 August 2023
Available online 25 August 2023

reported a bacteria-embedded poly-lactic-acid (PLA) capsule to improve the autonomous self-healing capacity of cementitious materials. The advantage of this capsule is that the PLA serves not only to protect the bacteria as a shell but also to provide the carbon source. It has been proved that the incorporation of PLA can significantly improve the self-healing capacity due to metabolic conversion of organic calcium salts by bacteria to calcium carbonate and carbon dioxide [18,19]. The metabolically produced carbon dioxide can react further with the alkalinity provided by the concrete matrix in the form of calcium hydroxide to produce more calcium carbonate.

Despite the prevalence of results on the performance of bacteria-based self-healing concrete, several key questions remain unanswered. Firstly, previous investigations have primarily evaluated crack healing by measuring the closure rate of surface-level cracks, with little attention paid to the extent of healing deeper within the cracks. Some researchers have even suggested that self-healing occurs only at the crack mouth [18–20], which appears inconsistent with the documented improvements in concrete durability resulting from bacteria-mediated limestone formation [21,22]. Secondly, as bacteria can only induce precipitation of calcium carbonate under specific environmental conditions, previous investigations have typically been conducted under the conditions that are ideal for bacterial growth but not realistic for most concrete structures. Research is thus necessary to evaluate the efficacy of self-healing under realistic environmental conditions. Thirdly, it is crucial that the healing agents containing bacteria should protect the bacteria during concrete mixing and hardening, while also being able to release the bacteria when cracking occurs. In the case of the PLA capsule, it functions through alkaline hydrolysis of PLA capsule to release bacteria when water enters a crack. However, the presence of water during concrete mixing also triggers the hydrolysis process, which may potentially damage the properties of concrete and therefore needs to be determined. This is important to ensure that the healing agent does not negatively affect the structural integrity of the concrete while at the same time can function as intended to promote self-healing.

To answer the above-mentioned questions, the current study investigated the crack-healing behaviour of mortar embedded with bacterial healing agents (*i.e.*, PLA capsules), in both short-term and long-term, under both ideal and realistic environmental conditions. Two sets of specimens were thus prepared and subjected to different healing regimes, with the first set kept in a mist room for varying short durations (*i.e.*, 1 week, 2 weeks, 3 weeks and 8 weeks) and the second set placed in an unsheltered outdoor environment for one year as a long-term healing investigation. Each set contained specimens with and without healing agents. To enable the observation of crack healing along crack depth, evolution of microstructure due to self-healing was characterized by BSE and EDS via the crack cross-sections, which also allows the examination of the PLA particles embedded in the mortar matrix. In the following sections, the design of the experimental program will first be introduced, followed by a detailed explanation of the sample preparation procedure, and the methods used to observe crack healing. Then, the progression of crack healing along crack depth for specimens with and without healing agents will be presented, starting with the short-term results, and concluding with the long-term results. Finally, the behaviour of individual PLA capsules during the healing process will also be discussed.

2. Materials and tests

2.1. Design of experiments

The experimental program of the current study has been designed such that the progress of crack healing over time can be observed at different crack width and under different healing regime. To facilitate the observation of healing at different crack width, the current study used dogbone-shaped specimens made of strain-hardening cementitious composite (SHCC) as shown in Fig. 1a and b. SHCC is a fibre-reinforced cement-based composite that exhibits multiple cracking behaviour under tension. This unique behaviour typically leads to the formation of closely spaced fine cracks with parallel crack walls. Unlike the V-shaped cracks created by bending tests, the parallel-wall cracks are beneficial for the investigation of healing due to the relatively uniform crack width along its depth. In addition, because of the inherent variability of the tensile properties, the cracks formed in the dogbone specimens usually have varied crack widths. The range of crack width that can be observed in a single dogbone specimen can be from a few microns to several hundreds of microns (Fig. 1c) and thus allows the observation of crack healing from the same specimen but at different crack width.

To study the crack-healing process under varying conditions, two sets of dogbone specimens were prepared as illustrated in Fig. 2. After cracking the specimens, the first set was kept in a mist room with saturated moisture and allowed to heal for various durations (ranging from one week to two months) as a short-term healing study. The second set was placed in an unsheltered outdoor environment and allowed to undergo a longer-term healing process for one year. Based on the meteorological history of the city (Delft) in which the experiments were carried out, there were 110 days with precipitation more than 1 mm and 20 days with daily low temperature below zero degree Celsius (Fig. 3). The specimens for long-term healing have thus experienced a considerable number of wet-dry cycles and freeze-thaw cycles. Specimens with

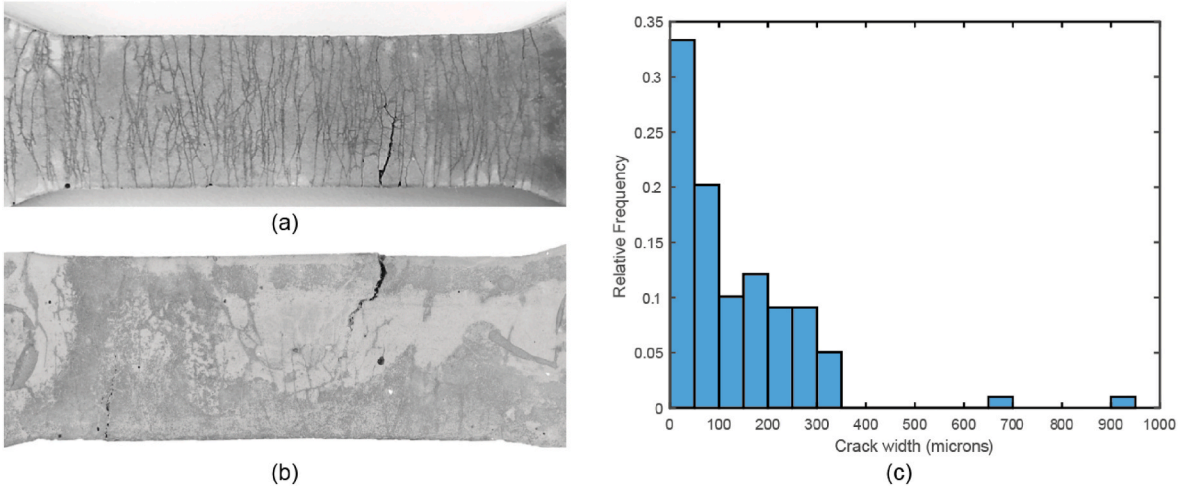

Fig. 1. Photograph of (a) a dogbone specimen of SHCC after uniaxial tension test and (b) a self-healed dogbone specimen; and (c) crack width distribution of the SHCC material adopted in the current study (calculated based on more than 8 specimens).

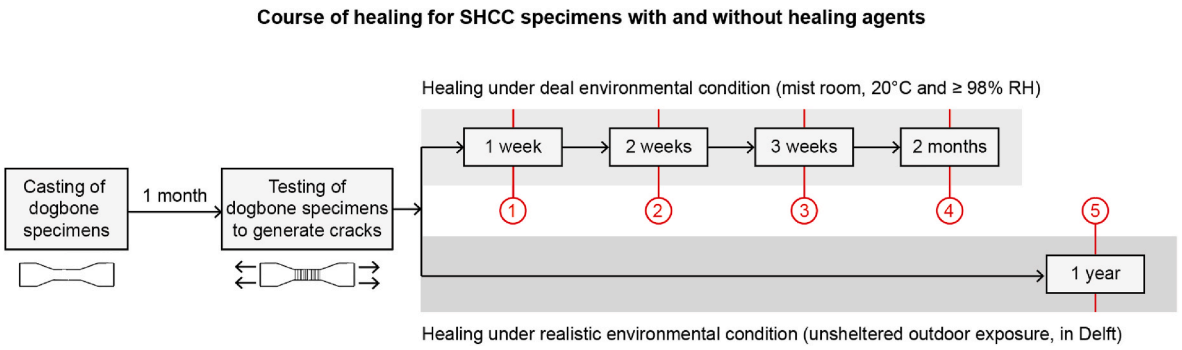

Fig. 2. Schematic illustration of experimental program.

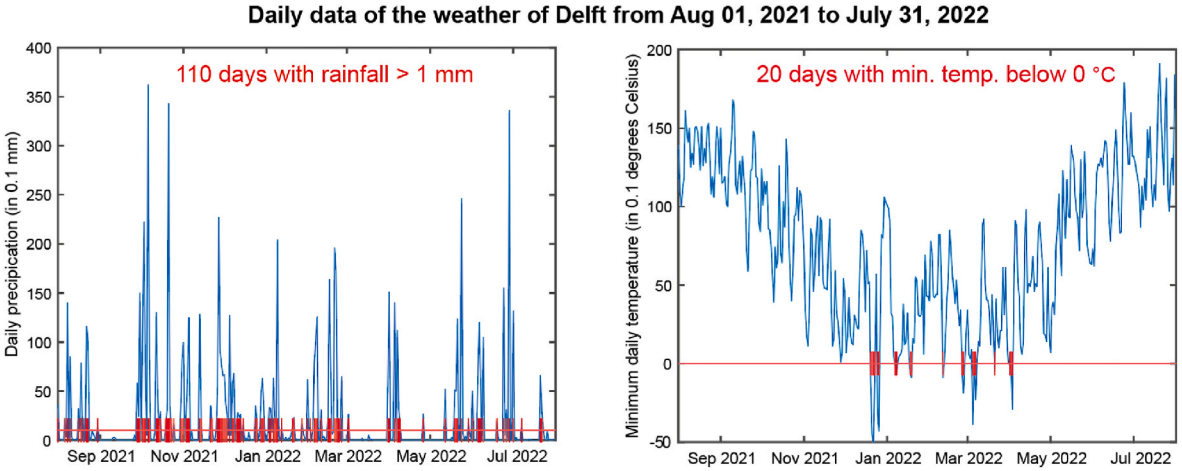

Fig. 3. Meteorological history of the experiment location (*i.e.*, Delft, the Netherlands). Data were obtained from the climate archive of Royal Netherlands Meteorological Institute (KNMI) data portal.

and without healing agent were both prepared for each set of experiments.

Microstructural characterization of crack healing was then carried out with segmented dogbone specimens as shown in Fig. 4a, with each segment having 3–5 penetrating cracks. The segments were then epoxy impregnated and coated to preserve the healing products precipitated both at the sample surface and inside the cracks. Characterization of crack healing along crack depth was then performed at the cross-sectional surfaces by cutting the epoxy coated segment from its middle (Fig. 4b). The detailed sample preparation procedure is given in the following sections.

Table 1
Mixture compositions of SHCCs [unit in kg/m^3].

Mixture ID	CEM III/B	Limestone powder	Water	SP	PVA fiber (2.0 vol %)	Healing agent (PLA capsule)
Reference SHCC	1060	530	424	2	26	0
Self-healing SHCC	1036	518	415	2	26	26

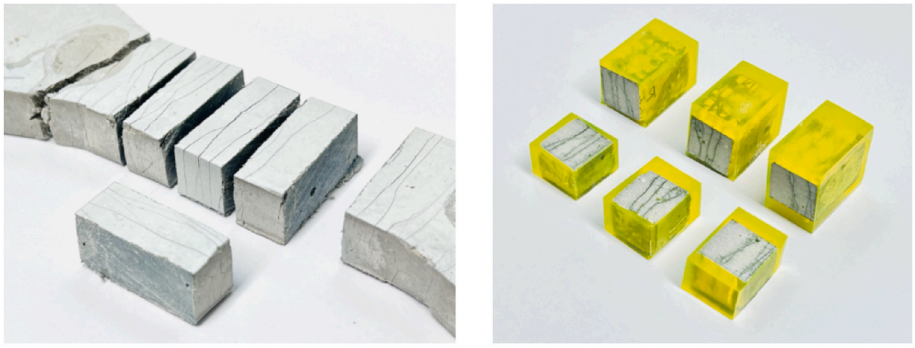

Fig. 4. Photograph of (a) cut segments from a dogbone specimen (gauge zone: 8 cm × 3 cm × 1.3 cm) and (b) epoxy impregnated specimens (3 cm × 1.3 cm × 1 cm).

2.2. Materials

Table 1 shows the mixture compositions of SHCC, which was developed previously [23]. The SHCC mixture has a water-to-binder ratio of 0.4 and a filler-to-binder ratio of 0.5. Blast furnace slag (BFS) cement CEM III/B 42.5 N from ENCI (the Netherlands), consisting of 20–34% clinker and 66–80% BFS [24], was used as binder. Finely grinded limestone powder Calcitec® from Carmeuse (Belgium) was used as filler. A polycarboxylate-based superplasticizer (SP) MasterGlenium 51 produced from BASF (Germany) with 35.0% solid content by mass was used to reach desired workability. The fibre used in this study is 8-mm-long polyvinyl alcohol (PVA) fibre from Kuraray (Japan) with 1.2% by weight oiling coating (fibre type: RECS15-8). The healing agents adopted in the current study are the bacteria-based polymeric particles produced by Green-Basilisk B.V. (the Netherlands). The particles are composed of a poly-lactic acid (PLA) derivate matrix, bacterial spores of *Bacillus cohnii* related strain (0.1–2% by weight) and growth-requiring nutrients. The capsules have a particle size distribution between 0.1 and 1.0 mm with a density of 1200 kg/m^3.

2.3. Sample preparation

To prepare the SHCC dogbone specimens, BFS cement and limestone powders were first dry mixed by a Hobart® mixer at low speed for 5 min. Water pre-mixed with 80% of SP was slowly added into the mixture and mixed until the fresh paste was homogenous and consistent. PLA capsules were then gradually added and mixed for another 2 min, followed by the addition of fibres within a duration of 5 min. Meanwhile, the remaining 20% SP was added into the mixture to compensate for the rheological loss due to the addition of fibres. Afterward, the fresh SHCC was cast into dogbone (80 mm × 30 mm × 13 mm in gauge length volume) moulds, while moderate vibration was applied to remove entrapped air and to improve consolidation. The moulds were then covered with plastic sheets and cured at room temperature for one day, after which the hardened specimens were removed from the moulds and cured in a climate room (20 °C and ≥98% RH) for another 27 days before tensile testing.

The hardened dogbone specimens first underwent uniaxial tension test to generate parallel micro-cracks within the neck. The uniaxial tensile tests were performed by using a servo-hydraulic testing machine (Instron® 8872) under displacement control at a rate of 0.005 mm/s. The tests were stopped when the applied tensile load dropped to 80% of the maximum load, and the load was then released. Directly after the generation of cracks by tensile test, the specimens were sawed into segments and then stored in different environments to initiate healing. The sawing process was carried out with great care to prevent secondary damage to the cracked specimen. Crack width measurement of selected cracks before and after sawing demonstrated that the sawing had minimal influence on the formed micro-cracks. At the end of their respective healing program, the specimens were removed from their designated environment and then dried in an oven at 40 °C for 2 days. Next, the segments were epoxy impregnated and coated to preserve the healing products precipitated both inside the cracks and at the sample surface and. To expose the cross-sectional surfaces, the epoxy-coated specimen was cut by a diamond saw from its middle. The exposed cross-section was then epoxy impregnated again to aid surface finishing. Afterward, the sample was first ground by 4000 grit abrasive papers for 5 min and then polished with a synthetic silk polishing cloth (MD-Dac from Struers) charged with 3 μm and 1 μm diamond paste for 2 separate 10-min-long sessions. An oil-based lubricant (DP-Lubricant Brown from Struers) was used to dissipate any heat built-up. Between each grinding/polishing interval, the sample was immersed in an ultrasonic bath for 30 s to remove debris from the surface.

2.4. Characterization methods

The polished cross-sections were characterized by backscattered electrons (BSE) imaging and energy dispersive X-ray spectroscopy (EDS). BSE analyses were carried out with the concentric backscattered (CBS) detector in an FEI QUANTA FEG 650 environmental scanning electron microscope (SEM) at high vacuum chamber condition. All specimens were coated with a layer of carbon of roughly 10 nm thick before BSE examination. Stitched BSE images of large area were taken with a commercial software (Maps 3 from Thermo Fisher Scientific). EDS elemental mapping was performed with the same SEM equipped with a silicon drift detector (SDD) with a NORVAR® light element window. The EDS maps were acquired by using the Pathfinder X-ray Microanalysis Software (Thermo Fisher Scientific). The combination of 50 μs dwell time per pixel with an averaging over 50 frames was found to provide good results. The resulting acquisition time of a map is around 30 min per area. All analyses (*i.e.*, BSE and EDS) were carried out at a working distance of 10 mm and at an accelerating voltage of 15 kV.

3. Results and discussion

3.1. Microstructural features of the specimens

Fig. 5 shows the typical appearance of a cross-section of the specimens under BSE. In the BSE images, the brightness of each pixel depends on the mean atomic number of the underlying phases. This allows different phases to be distinguished based on their grayscale. The epoxy filled cracks can be easily identified in the graph as dark lines penetrating the whole specimen horizontally. The left and right sides of the specimen are respectively the top and bottom exposing surfaces of the original dogbone specimen as shown in Fig. 4a. In addition to cracks, epoxy filled pores could be seen also in dark black, leading to shadowy appearance in areas with a high porosity. Embedded fibres and PLA capsules, which both contain mainly the element of carbon, can also be found as regions in dark back. They can be distinguished by their shape, with fibres appearing as either circular or oval and PLA capsules appearing an irregular shape. Some large black circles can also be seen, which are epoxy filled air voids.

In the following sections, characterization of the crack healing will first focus on the crack mouths located at either left or right side of the specimens (marked as red squares, such as Fig. 5b). The extent to which healing occurred along crack depth will be determined by shifting the focus from the crack mouths to the middle of the specimen. Moreover, the microstructure of matrix that surrounds crack-passing PLA particles (marked as green squares, such as Fig. 5c) will be analysed to reveal the mechanism by which the PLA particles contribute to the healing of cracks.

3.2. Process of crack-healing over time

3.2.1. Short-term healing under controlled climate

Fig. 6 shows the BSE images taken at crack mouth from specimens amended with healing agent. These specimens were kept in a mist room after cracking and were incubated for various short durations (ranging from 1 week to 8 weeks) as a short-term healing study. As can be seen, no trace of healing was observed after the 1st week, even for cracks as small as 7 μm. At the end of the 2nd week, precipitates began to form near crack mouths, preferably covering the entrance of the cracks instead of filling them. The precipitates formed presumably due to bacterial conversion of PLA-derived calcium lactate to calcium carbonate. At this moment, only cracks smaller than 20 μm were observed to experience certain degree of healing (Fig. 6d). Deposition of minerals around crack mouths of larger cracks were also observed; but these minerals mainly accumulated near the tips of crack walls instead of bridging over the crack (Fig. 6c). At the end of the 3rd week, the extent of crack healing was noted to progress considerably, with cracks as large as 80 μm being

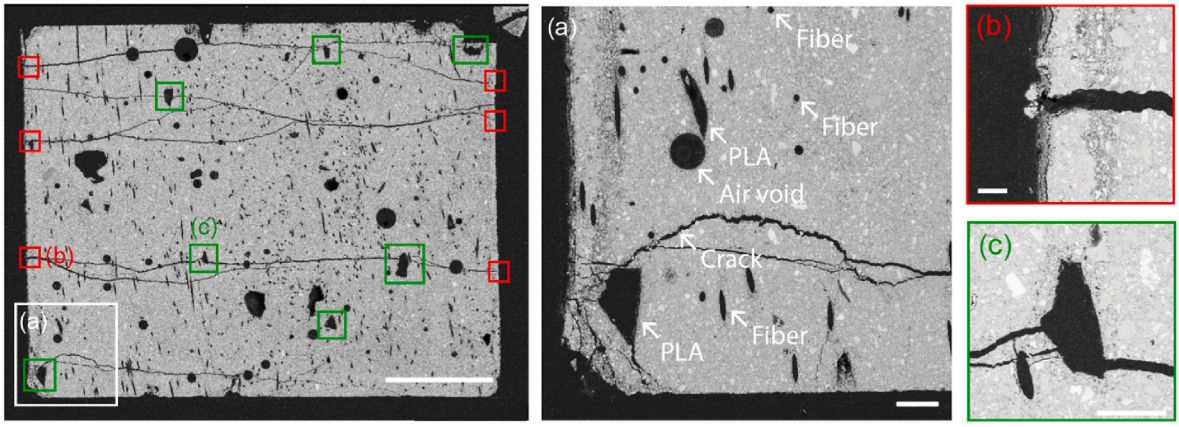

Fig. 5. Stitched BSE micrograph of a cross-section (scale bar = 3 mm) of a cracked and healed SHCC segment: (a) the bottom left corner (scale bar = 300 μm), (b) a crack mouth (scale bar = 100 μm) and (c) a bacteria-embedded PLA particle (scale bar = 200 μm).

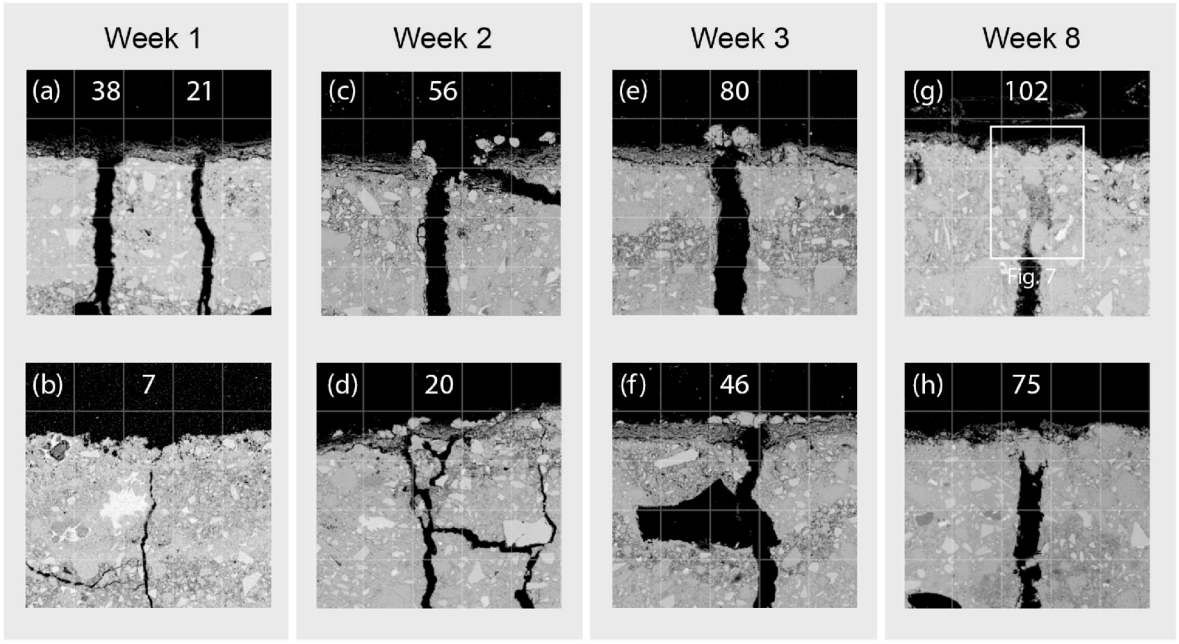

Fig. 6. Progress of crack healing over time at crack mouth in specimens with healing agents. Each image captures a region of 500 μm × 500 μm. Grids are provided for easy estimation of crack width and precipitate size. Each cell in grids is 100 μm × 100 μm. The number in each figure is the crack width in the unit of micron.

covered fully by precipitates (Fig. 6e). The size of the individual precipitate was also found to increase from roughly 20–30 μm at the end of the 2nd week to around 70–80 μm at the end of the 3rd week. The observation by now is in line with our understanding on the characteristic of the aerobic bacterial activity, which is that this biochemical reaction through which calcium lactate is converted to calcium carbonate depends on the availability of oxygen. Therefore, the precipitation of minerals should start at the locations where oxygen abounds.

Significant changes were noticed after longer incubation duration (*i.e.*, 8 weeks). Not only even larger cracks were found to heal (Fig. 6g), but also the precipitates which were previously only grouping over crack mouths started to form inside the cracks. As showed by Fig. 7, EDS element mappings reveal that the formed precipitate inside the cracks was an association of calcium, oxygen and carbon elements, which suggests that mineral precipitates were indeed calcium carbonate based. Fig. 8 shows a comparison of the crack cross-sections after 3-week healing and 8-week healing (extended view of Fig. 6f and h). As can be seen, at the end of the 3rd week, the crack walls were still smooth and barely any crystals or healing products can be found inside the crack; on the contrary, the cracks after 8-week healing appeared to have crystals precipitated at both crack walls as deep as 1.5 mm inside the crack. EDS element mappings indicate that the precipitates were likely calcium carbonate, since no silicon, sulphur and aluminium were detected, which rules out the possibility of CSH, ettringite or AFm. The precipitates appeared to be a mixture of calcite and aragonite, displayed primarily as rhombohedra and needle in shape. To further investigate the morphology of the precipitates, a healed specimen without epoxy impregnation was opened through a crack to examine the crystals formed inside. Fig. 9a shows the BSE image of one crack surface with the bottom edge being the entrance of the crack. Fibres can also be found protruding out from the matrix. As can be seen, a large number of crystals can be found on the crack surface (Fig. 9b). Rhombohedral crystals with somewhat rounded edges and surface indentations of bacteria encased within the growing crystals (Fig. 9c) were observed closer to crack mouth. Further away from the crack entrance, needle-shape crystals were found to dominate (Fig. 9d). Similar to what was seen in Fig. 8, the depth to which the precipitates were found inside a crack was within 2 mm. It also appears that the size of crystals was larger

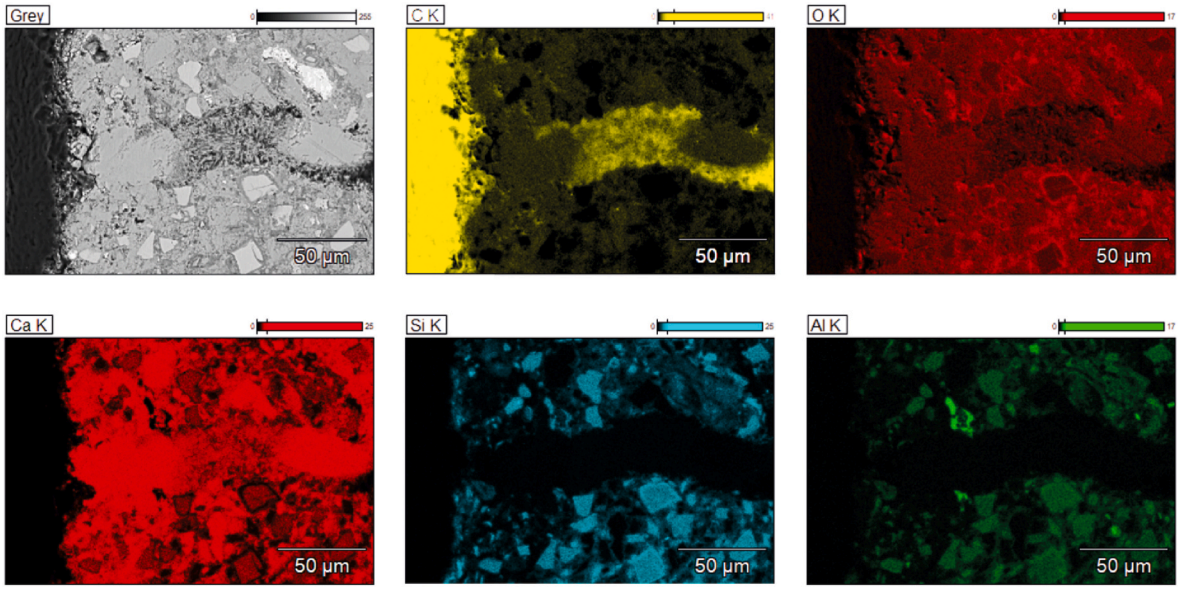

Fig. 7. EDS elemental mappings of a healed crack mouth after 8 weeks of healing in a mist room from a specimen with healing agents. The location of this mapping is marked in Fig. 6 as a white rectangle.

when they were close to the crack mouth.

The delayed formation of calcium carbonate inside a crack as compared to the calcium carbonate formed at crack mouth again highlights the importance of the oxygen availability. Since bacteria and organic carbon are embedded inside the healing agent capsules, one would have expected that healing should occur first inside a crack, preferably close to a healing particle. However, as what has been shown by the BSE images, the formation of healing products inside a crack occurred several weeks later than the healing at crack mouth. The underlying cause may be attributed to a dual-factor phenomenon. Firstly, the initial oxygen content inside a crack is limited due to the fact that the oxygen can only be supplied via cracks and that the slag containing cement-based matrix itself also consumes oxygen when a crack forms. This is because that the formation of metal sulphides such as FeS and MnS during hydration under anoxic conditions will also react with oxygen whenever oxygen becomes available, through which the S^{2-} ions are oxidized into $S_2O_3^{2-}$ (intermediate) and SO_4^{2-} (stable) ions. Secondly, the formation of the calcium carbonate at the crack mouth will inevitably block the ingress of oxygen, which further limits oxygen availability in cracks and decreases the rate of calcium carbonate precipitation.

Figs. 10 and 11 document the autogenous crack healing process of the reference SHCC specimens without healing agent. As can be seen, evident crack closure occurred after a period of 3 weeks in a humid environment. Similar to the bacteria-enabled healing process, healing products started to precipitate from the two sides of a crack mouth and then gradually bridged over the crack mouth by accumulating more crystals. At the end of the 8th week, cracks around 100 μm wide were observed to heal completely. The healing product is expected to be also calcium carbonate but was formed due to carbonation with the carbon dioxide from the environment. By comparing Figs. 10 and 6, it can be seen that autogenous healing happens slower than the bacteria-enabled healing. The size of the crystals formed due to autogenous healing also appear to be smaller than the crystals formed in bacterial samples. Crack width was found to be a controlling factor for both autogenous and bacteria-enabled healing, as smaller cracks always healed faster than larger ones. However, crack width does not seem to influence the size and the morphology of the precipitated crystals. Another distinction between the two types of healing is the healing condition inside the crack. Unlike the specimens with healing agent (Fig. 8), no crystals can be observed inside a crack in specimens without healing agent (Fig. 12). This agrees with previous study which utilized X-ray computed microtomography to study autogenous healing of cementitious material [25]. It was found that, even under the condition of wet–dry cycles, the crack is closed by calcium carbonate formation only near the crack mouth.

3.2.2. *Long-term healing under natural exposure*

Fig. 13 shows the microstructure of a specimen with healing agent after one year exposure in an unsheltered outdoor environment. As can be seen, the distribution of healing products in Fig. 13 is essentially different than in specimens that have undergone short-term healing. While the most obvious crack closure happened close to crack mouth after short-term healing, the precipitation of healing products after a long-term healing is found to occur predominantly near a healing particle. As can be seen from the BSE image, epoxy filled cracks gradually disappeared when approaching a healing agent particle. If the healing process can only result in the relocation of calcium element, the microstructure of an area before and after the precipitation of calcium carbonate can then be compared by assessing the silicon mapping and the calcium mapping. From the silicon mapping, it can be seen that the original boundary of the healing agent was smooth and that several cracks passed through the healing agent; and the calcium mapping revealed that the outer layer of the particle was consumed and converted to a calcium-rich rim, resulting in a rough boundary of healing agent. Also, the cracks which were originally passing through the particles were filled and even air voids were partially filled by the precipitates. This microstructural change indicates that, after one year of outdoor exposure, oxygen seems to have entered so deep that there is enough oxygen for the bacteria around a particle to become active. The availability of oxygen is thus no longer governing the metabolic activities of the bacteria in this case. In addition, it can also be found that no healing products can be seen at crack mouth. Since the specimens were placed outdoor for a whole year in a climate where temperature can drop below freezing point in winter, it is possible that the environmental actions such as rainfall and freeze and thaw cycles may have worn away the healing products at the crack mouth [21] and thus led to a deeper ingress of oxygen into cracks, which promoted the bacteria to precipitate preferably near a healing agent.

Fig. 14 shows BSE images of 2 different locations in the bacterial specimens after long-term healing, both of which show evident healing along the crack walls extending several millimetres deep inside the cracks. As the thickness of the specimen is 13 mm, the observed 6-mm-

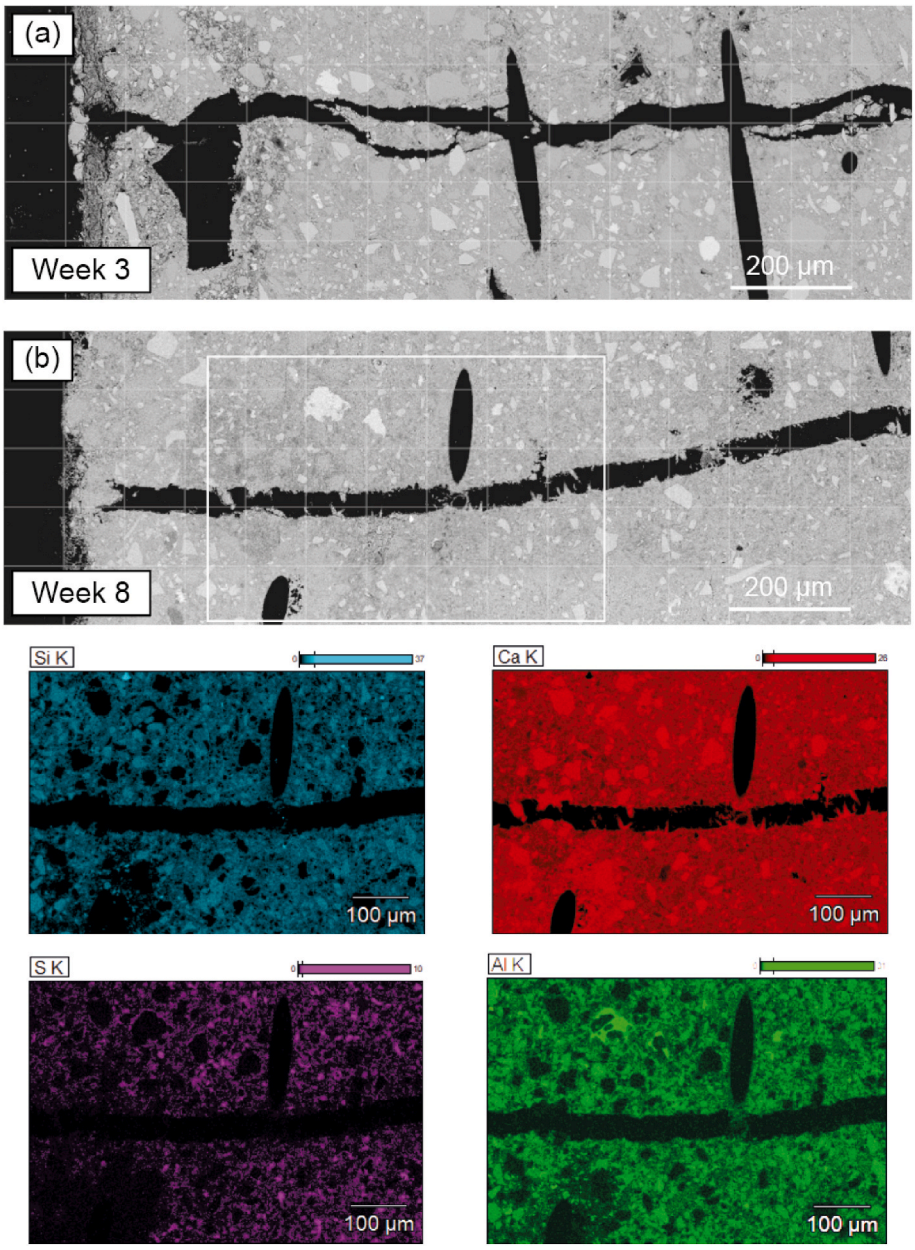

Fig. 8. Comparison of the depth of healing occurred inside a crack after a period of (a) 3 weeks and (b) 8 weeks in a mist room for specimens with healing agent (width of field = 1.5 mm).

deep healing from one side of the specimen means that the entire crack path has undergone certain degree of healing. By comparing the silicon mapping and calcium mapping, it can be seen that the precipitated calcium carbonates have filled the small cracks, narrowed the larger ones, and partially filled some voids. It is also interesting to notice that all the healing agent particles which were activated by cracks had the outer layer converted into calcium carbonate, which may have restricted the further hydrolysis of the PLA and thus limited the discharge of bacterial spores. This self-limiting feature can have both negative and positive consequences. At one hand, it will certainly impede the pace of crack-healing by limiting the amount of spores and nutrients released by each particle. On the other hand, the preservation of certain portion of the particle can produce a repeated healing, when the material is damaged again. Therefore, the particle size of healing agent can be an important factor and should be designed according to the expected crack width and the specific working condition.

Fig. 15a shows the microstructure of a reference specimen after 1-year autogenous healing. The autogenous healing capacity of SHCC is evident from the observed crack closure near the crack exit on both the smaller and larger cracks. Similar to the specimens with healing agent, no precipitates were observed at the crack mouth. This may also because of the environmental effects acting upon the healing products. However, a key difference between autogenous and autonomous healing is the depth to which the crack can be healed. In the bacterial specimen (Fig. 14), precipitation of calcium carbonate along the crack walls was clearly visible, while obvious narrowing of cracks due to calcium carbonate precipitation occurred only within 0.5 mm deep in the reference specimen (Fig. 15b). This may be because even if the precipitates at the crack mouth were gone, the ingress of carbon dioxide would still be blocked by the calcium carbonate formed slightly deeper in the cracks, as long as this affected zone is within the carbonation front. Consequently, the availability of carbon dioxide for autogenous healing was still limited, resulting in only a very thin layer of calcium-rich precipitates along the crack walls, as shown in Fig. 15c (processed calcium

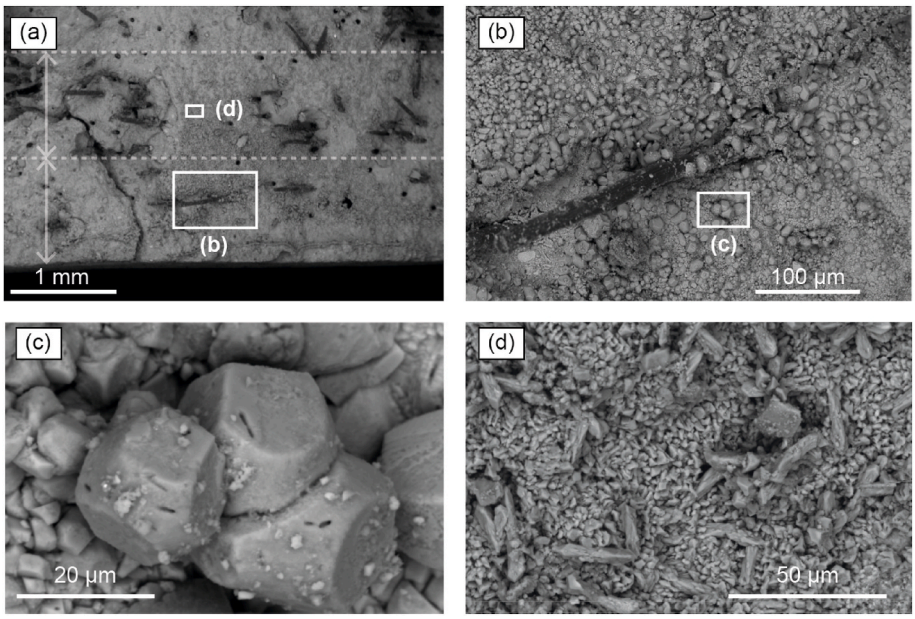

Fig. 9. Morphology of precipitated healing products inside a crack after an 8-week-long healing process.

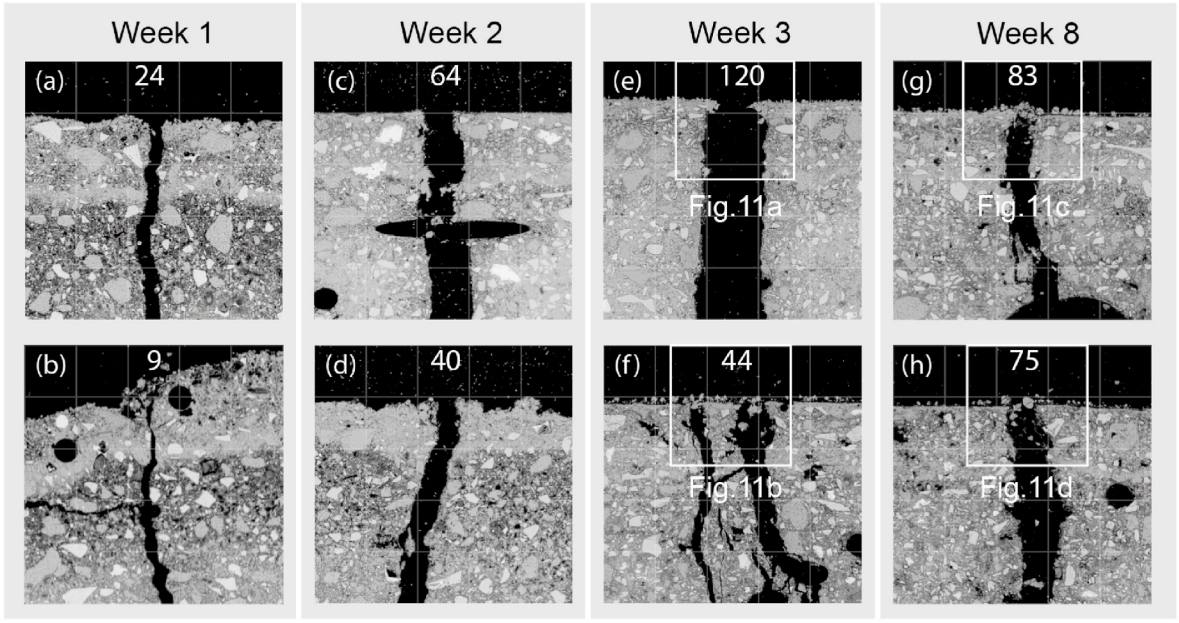

Fig. 10. Process of autogenous crack healing at crack mouth in refence specimens without healing agents. Each image captures a region of 500 μm × 500 μm. The number in each figure is the crack width in the unit of micron.

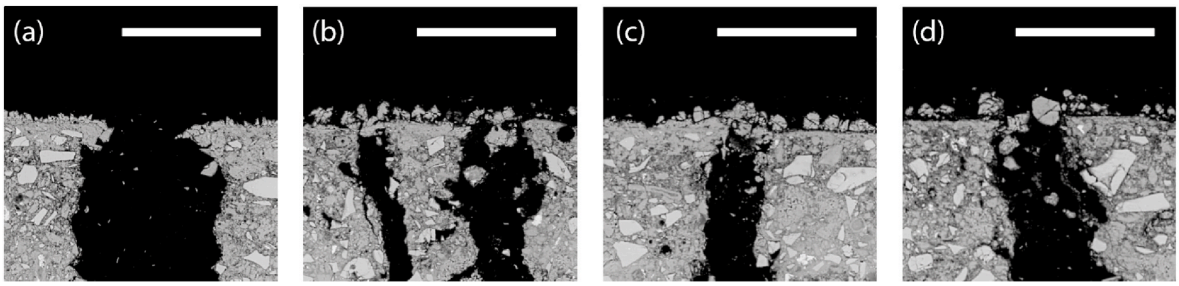

Fig. 11. Zoom-in views of autogenous healing at crack mouth of reference specimens at (a–b) week 3 and (c–d) week 8 (scale bar = 100 μm).

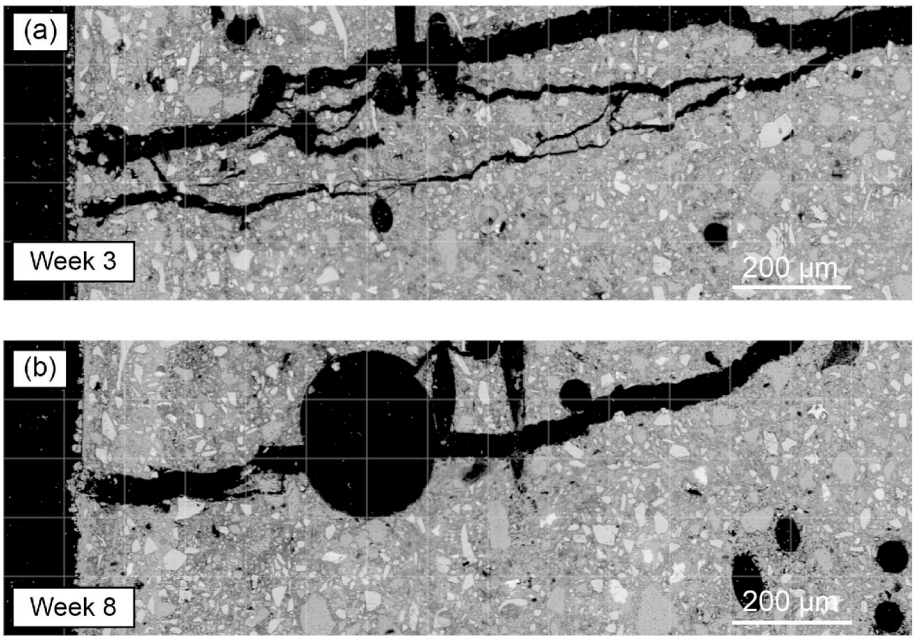

Fig. 12. Comparison of the autogenous healing occurred inside a crack after a period of (a) 3 weeks and (b) 8 weeks in mist room for the reference specimens without healing agent (width of field = 1.5 mm).

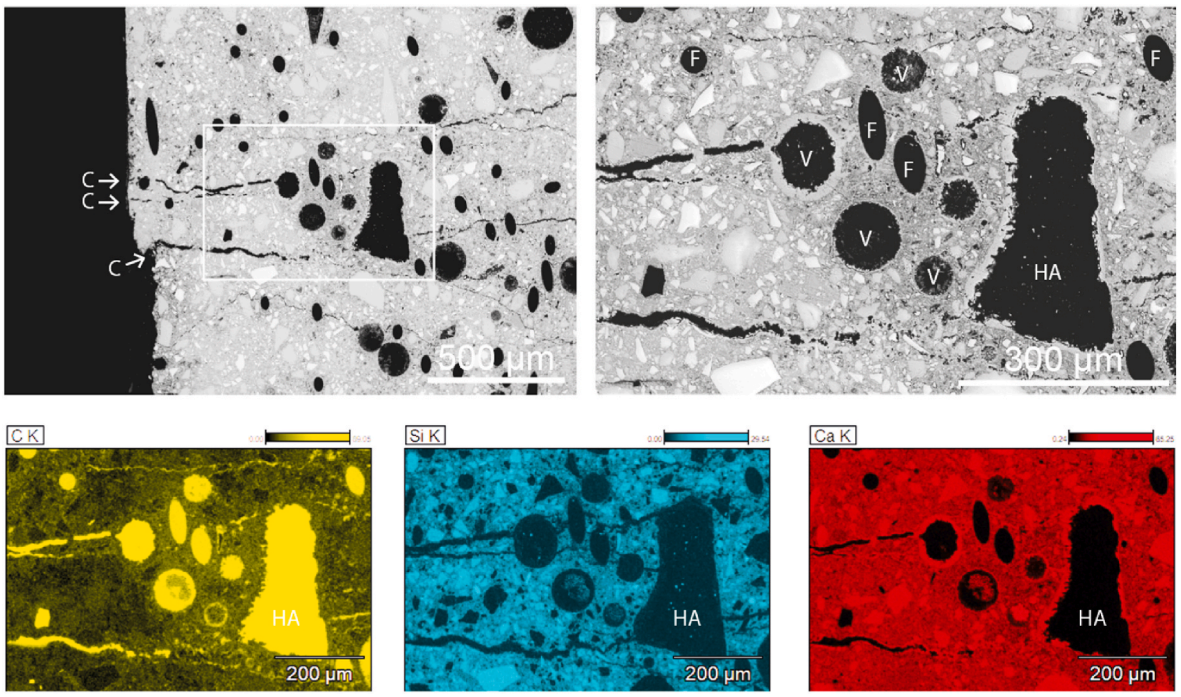

Fig. 13. BSE images and EDS mappings of a specimen with healing agents after 1-year outdoor exposure. (Abbreviation: C – crack; F – fibre; V – void; HA – healing agent).

mapping depicting only high-intensity calcium signals).

By comparing the extend of healing observed in the specimens with and without healing agents, it can be concluded that the use of aerobic bacteria is highly beneficial in terms of crack healing, for that the bacteria have changed the governing factor for the yield of calcium carbonate deep inside the cracks from the availability of carbon dioxide to the availability of oxygen. And since oxygen diffuses more easily in concrete than carbon dioxide, this change of limiting factor increases the likelihood of calcium carbonate precipitation in deeper cracks. Moreover, the metabolic activities of aerobic bacteria also produce carbon dioxide, which can react with calcium hydroxide minerals in locations that are not accessible to carbon dioxide from the outside atmosphere.

Another conclusion that can be drawn from this study is that relying solely on the observation of the crack mouth to evaluate crack sealing or healing may not be a reliable method. This is evident from the BSE images of the crack cross-sections, which show that a complete closure of crack mouth can occur even when there is essentially no healing occurring inside the crack. Conversely, the absence of healing products at the crack mouth does not necessarily indicate a lack of healing inside the crack. Certainly, the discussion of healing efficiency should come

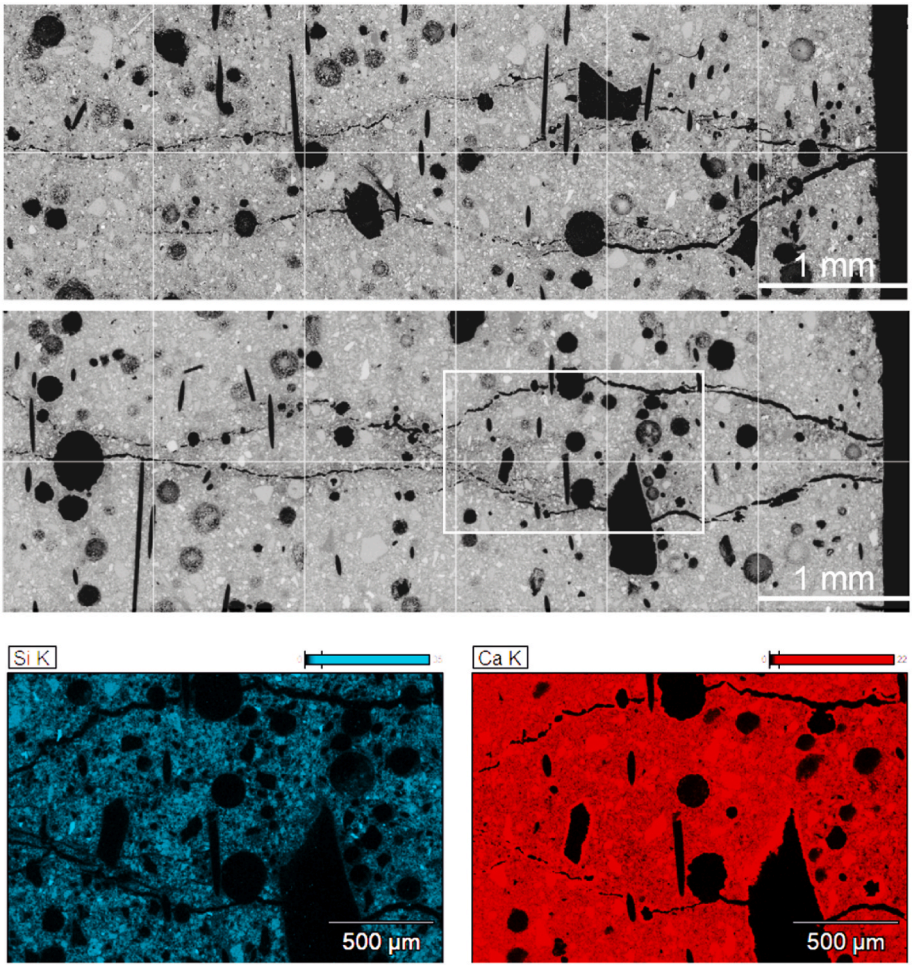

Fig. 14. BSE images of 2 different locations in a specimen with healing agents after 1-year outdoor exposure, showing evident healing along crack depth (width of field = 6 mm).

after the establishment of the demand from healing.

3.3. Behaviour of bacteria-embedded PLA capsules in cement-based matrix

In the development of all types of self-healing concrete, it is important to ensure that the healing agent does not affect too much the properties of concrete and at the same time can still function as intended to promote self-healing. The PLA capsule adopted in the current study functions through hydrolysis of the PLA to release bacteria when water enters a crack. However, the presence of water during concrete mixing is expected to trigger the hydrolytic degradation of PLA already from the start. Depolymerization via hydrolysis leads to the formation of lactic acid, which consumes some alkalinity in concrete close to the PLA capsule. It is therefore necessary to verify if PLA particles can modify the microstrucutre of cement-based matrix surrounding it.

Fig. 16 shows the BSE images of two PLA particles embedded in the specimens at a very early stage after cracking (*i.e.*, at the end of the 1st week). As can be seen, a porous zone can indeed be noticed surrounding the particles. The thickness of this zone is around 50 μm, which is the typical thickness of the interfacial transition zone (ITZ) between a bigger inclusion and cement-based matrices [26,27]. In fact, similar porous zone can also be seen around the circular air void at the top right corner of Fig. 16c and d, which suggests that the influence of the PLA to its surrounding matrix is only minor, and that the hydrolytic degradation of PLA may have only happened to a very limited extent. Conversely, the hydrolysis of PLA during the self-healing process is quite noticeable. As shown by Figs. 17 and 3 weeks in a mist room has led to the formation of a calcium-rich rim around the particle. It is likely that the reaction between the lactic acid and the calcium hydroxide in the matrix has led to the formation of calcium lactate, which might have been metabolically converted into calcium carbonate and filled the cracks next the particle. At this moment, the ITZ between the particle and the cement-based matrix also appeared to be less porous, probably also due to the precipitated calcium carbonate. Fig. 18 shows the typical appearance of a PLA particle inside a crack after 8 weeks of healing. By comparing the silicon mapping and the calcium mapping, it can be seen that almost 1/3 of the particle has now been consumed and converted into calcium rich precipitates either around the particle or close to the crack mouth. The porous zone surrounding the particle is also no longer visible. It is thus concluded that the bacteria-embedded healing particles can indeed function as intended to promote self-healing, while posing no threat to the concrete properties.

4. Conclusions

An experimental study was carried out to characterize the bacteria-enabled crack-healing behaviour of mortar by BSE and EDS. Healing under both short-term ideal condition and long-term realistic condition were investigated. Unlike previous studies which usually quantify healing by examining the formation of healing products at crack mouth, the current study documented the process of both autogenous and autonomous healing along crack depth. The behaviour of individual PLA capsules during the healing process was also studied. The main findings

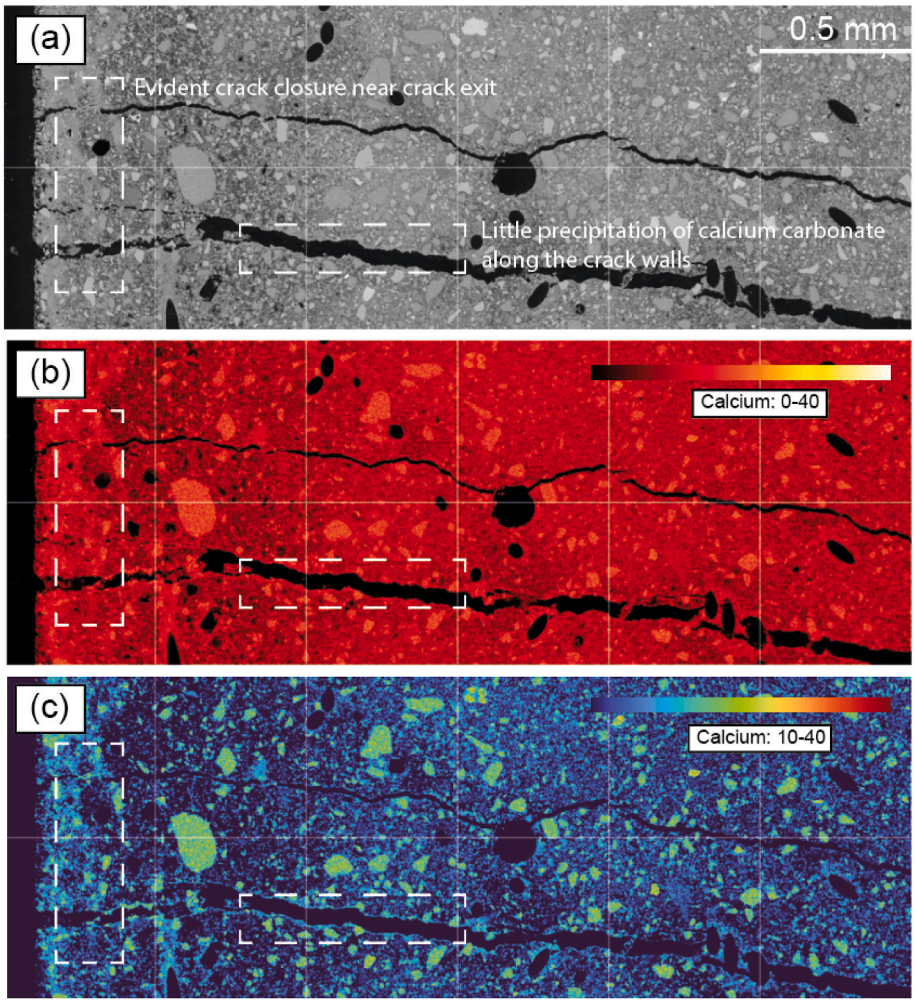

Fig. 15. (a) BSE image of a reference specimen without healing agents after 1-year outdoor exposure showing limited healing along crack walls (width of field = 6 mm) and (b) EDS mapping of calcium element and (c) processed calcium mapping showing only locations where high intensity calcium signal was detected.

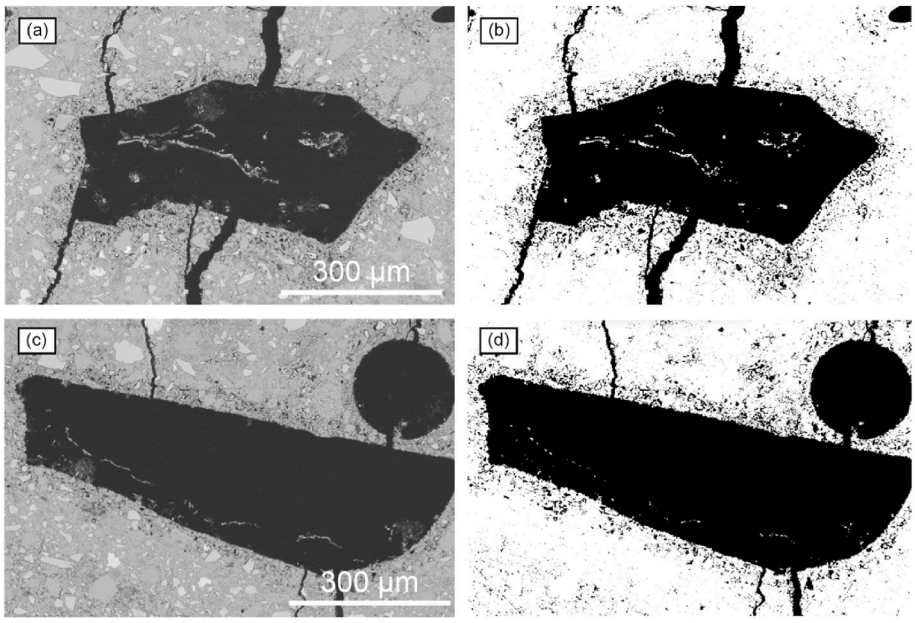

Fig. 16. BSE images of crack-bridging PLA particles after a period of 1 week in mist room as well as their respective binary images highlighting porosity after grayscale segmentation.

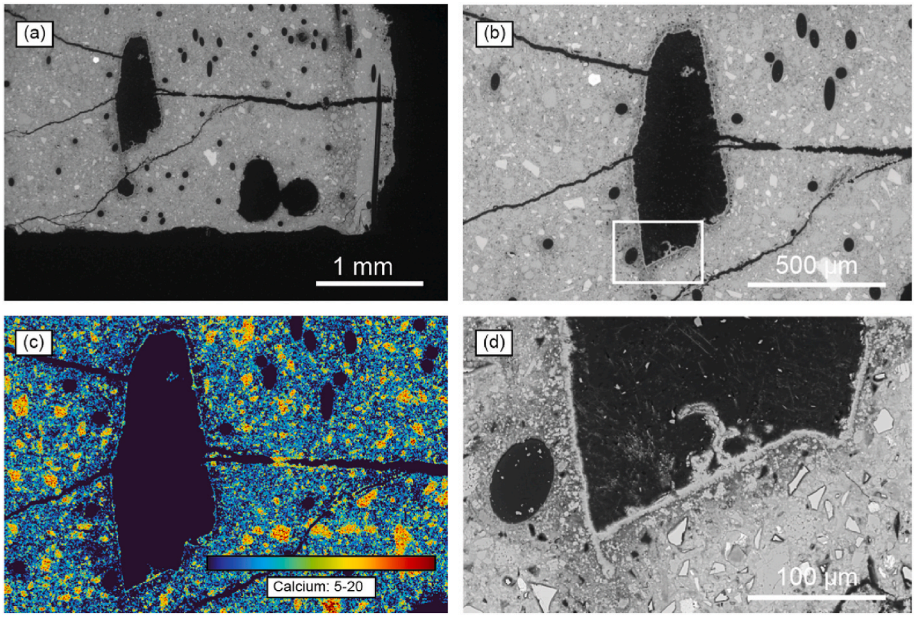

Fig. 17. BSE images of a crack-bridging PLA particle after a period of 3 weeks in mist room as well as its EDS calcium mapping.

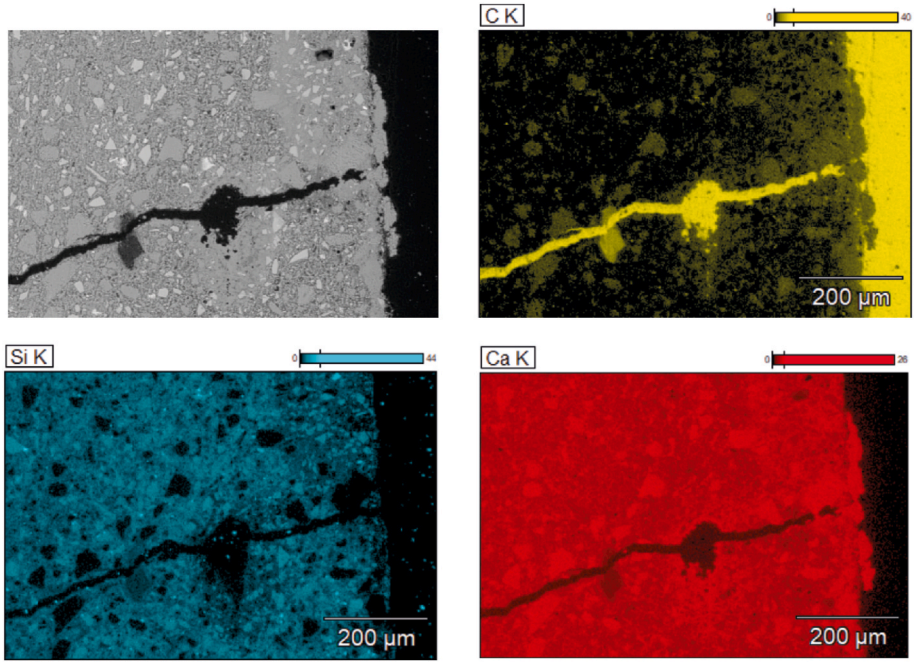

Fig. 18. BSE image and EDS mappings of a crack-bridging PLA particle after 8 weeks in mist room.

of the current study are:

1. Apparent crack healing enabled by bacteria began after 2 weeks in a humid environment. The healing products initially precipitated at the crack mouth and gradually moved deeper into the cracks, with the precipitated crystals growing larger over time. After a period of 8 weeks, cracks as wide as 100 µm were fully filled with healing products at the crack mouth. Healing products were also found to form a few millimetres deep inside the crack.
2. Autogenous healing happened slower than the bacteria-enabled healing. Only after the end of the 3rd week, healing products started to precipitate from the two sides of a crack mouth and then gradually bridged over the crack mouth by accumulating more crystals. Despite a slower speed, cracks of 100 µm wide were also observed to heal completely at the end of the 8th week. However, healing products were only found at crack mouth, leaving the crack depth largely unhealed.
3. Long-term crack healing in realistic environment was observed to fundamentally differ from healing under short-term controlled conditions. Specimens with healing agent were found to have no healing products formed at the crack mouth but have a high degree of healing through the entire crack depth. It is likely that the environmental actions such as rainfall and freeze and thaw cycles may have worn away the healing products at the crack mouth and thus led to a deeper ingress of oxygen into cracks, which promoted the aerobic metabolic activity of the bacteria inside the cracks.

4. Autogenous healing after long-term outdoor exposure was found to possess similar characteristics, with the depth of healing increased and a loss of healing products at surface. However, the depth to which a crack can heal because of autogenous healing is significantly less than bacterial healing, which is probably due to the limited ingress of carbon dioxide inside the cracks.
5. The cement-based matrix surrounding a PLA particle was found to be porous. This porous zone appeared to be similar to the ITZ commonly formed between cement-based matrices and big inclusions such as fibres and aggregates, which suggests that the hydrolytic degradation of PLA may have only happened to a very limited extent during concrete mixing and hardening.
6. During the healing process, the PLA particles were found to be consumed and converted into calcium-rich precipitates, potentially calcium carbonate. The formed calcium carbonate can not only heal the cracks but also densify the matrix surrounding the healing agents.
7. Relying solely on the observation of crack mouths to evaluate crack sealing or healing may not be a reliable method. This is evident from the BSE images of the crack cross-sections, which show that a complete closure of the crack mouth can occur even when there is essentially no healing occurring inside the crack. Conversely, the absence of healing products at the crack mouth does not necessarily indicate a lack of healing inside the crack.

Declaration of competing interest

The authors declare that they have no known competing financial interests or personal relationships that could have appeared to influence the work reported in this paper.

Data availability

Data will be made available on request.

Acknowledgement

Shan He acknowledges the financial supports from the MSCA-ITN project SMARTINCS. This project has received funding from the European Union's Horizon 2020 research and innovation programme under the Marie Skłodowska-Curie grant agreement No 860006. Zhi Wan would like to acknowledge the funding supported by China Scholarship Council under grant number 201906220205. In addition, the authors would like to thank Green-Basilisk B.V. for providing the healing agent (*i.e.*, the bacteria-embedded polylactic acid capsules).

References

[1] E. Schlangen, S. Sangadji, Addressing infrastructure durability and sustainability by self healing mechanisms - recent advances in self healing concrete and asphalt, in: Procedia Eng, Elsevier Ltd, 2013, pp. 39–57, https://doi.org/10.1016/j.proeng.2013.03.005.
[2] Y. Yang, M.D. Lepech, E.H. Yang, V.C. Li, Autogenous healing of engineered cementitious composites under wet–dry cycles, Cement Concr. Res. 39 (2009) 382–390, https://doi.org/10.1016/J.CEMCONRES.2009.01.013.
[3] K. Van Tittelboom, N. De Belie, Self-healing in cementitious materials-a review, Materials 6 (2013) 2182–2217, https://doi.org/10.3390/ma6062182.
[4] G. Yildirim, Ö.K. Keskin, S.B.I. Keskin, M. Şahmaran, M. Lachemi, A review of intrinsic self-healing capability of engineered cementitious composites: recovery of transport and mechanical properties, Construct. Build. Mater. 101 (2015) 10–21, https://doi.org/10.1016/J.CONBUILDMAT.2015.10.018.
[5] H. Huang, G. Ye, D. Damidot, Effect of blast furnace slag on self-healing of microcracks in cementitious materials, Cement Concr. Res. 60 (2014) 68–82, https://doi.org/10.1016/J.CEMCONRES.2014.03.010.
[6] C. de Nardi, S. Bullo, L. Ferrara, L. Ronchin, A. Vavasori, Effectiveness of crystalline admixtures and lime/cement coated granules in engineered self-healing capacity of lime mortars, Mater. Struct. 50 (4) (2017) 1–12, https://doi.org/10.1617/S11527-017-1053-3, 50 (2017.
[7] L. Ferrara, V. Krelani, M. Carsana, A "fracture testing" based approach to assess crack healing of concrete with and without crystalline admixtures, Construct. Build. Mater. 68 (2014) 535–551, https://doi.org/10.1016/J.CONBUILDMAT.2014.07.008.
[8] D. Snoeck, K. Van Tittelboom, S. Steuperaert, P. Dubruel, N. De Belie, Self-healing cementitious materials by the combination of microfibres and superabsorbent polymers, J. Intell. Mater. Syst. Struct. 25 (2012) 13–24, https://doi.org/10.1177/1045389X12438623.
[9] J.Y. Wang, H. Soens, W. Verstraete, N. de Belie, Self-healing concrete by use of microencapsulated bacterial spores, Cement Concr. Res. 56 (2014) 139–152, https://doi.org/10.1016/J.CEMCONRES.2013.11.009.
[10] T. Van Mullem, G. Anglani, M. Dudek, H. Vanoutrive, G. Bumanis, C. Litina, A. Kwiecień, A. Al-Tabbaa, D. Bajare, T. Stryszewska, R. Caspeele, K. Van Tittelboom, T. Jean-Marc, E. Gruyaert, P. Antonaci, N. De Belie, Addressing the need for standardization of test methods for self-healing concrete: an inter-laboratory study on concrete with macrocapsules, Sci. Technol. Adv. Mater. 21 (2020) 661–682, https://doi.org/10.1080/14686996.2020.1814117.
[11] Y. Shields, N. de Belie, A. Jefferson, K. van Tittelboom, A review of vascular networks for self-healing applications, Smart Mater. Struct. 30 (2021), 063001, https://doi.org/10.1088/1361-665X/ABF41D.
[12] H.M. Jonkers, A. Thijssen, G. Muyzer, O. Copuroglu, E. Schlangen, Application of bacteria as self-healing agent for the development of sustainable concrete, Ecol. Eng. 36 (2010) 230–235, https://doi.org/10.1016/J.ECOLENG.2008.12.036.
[13] V. Wiktor, H.M. Jonkers, Quantification of crack-healing in novel bacteria-based self-healing concrete, Cem. Concr. Compos. 33 (2011) 763–770, https://doi.org/10.1016/J.CEMCONCOMP.2011.03.012.
[14] J.Y. Wang, H. Soens, W. Verstraete, N. De Belie, Self-healing concrete by use of microencapsulated bacterial spores, Cement Concr. Res. 56 (2014) 139–152, https://doi.org/10.1016/J.CEMCONRES.2013.11.009.
[15] Y.C. Ersan, D. Palin, S.B. Yengec Tasdemir, K. Tasdemir, H.M. Jonkers, N. Boon, N. De Belie, Volume fraction, thickness, and permeability of the sealing layer in microbial self-healing concrete containing biogranules, Front Built Environ 4 (2018) 70, https://doi.org/10.3389/FBUIL.2018.00070/BIBTEX.
[16] E. Tziviloglou, V. Wiktor, H.M. Jonkers, E. Schlangen, Selection of nutrient used in biogenic healing agent for cementitious materials, Front Mater 4 (2017), https://doi.org/10.3389/fmats.2017.00015.
[17] R.M. Mors, H.M. Jonkers, Feasibility of lactate derivative based agent as additive for concrete for regain of crack water tightness by bacterial metabolism, Ind. Crops Prod. 106 (2017) 97–104, https://doi.org/10.1016/j.indcrop.2016.10.037.
[18] R. Roy, E. Rossi, J. Silfwerbrand, H. Jonkers, Self-healing capacity of mortars with added-in bio-plastic bacteria-based agents: characterization and quantification through micro-scale techniques, Construct. Build. Mater. 297 (2021), 123793, https://doi.org/10.1016/J.CONBUILDMAT.2021.123793.
[19] E. Rossi, R. Roy, O. Copuroglu, H.M. Jonkers, Influence of self-healing induced by polylactic-acid and alkanoates-derivates precursors on transport properties and chloride penetration resistance of sound and cracked mortar specimens, Construct. Build. Mater. 319 (2022), 126081, https://doi.org/10.1016/J.CONBUILDMAT.2021.126081.
[20] K. Sisomphon, O. Copuroglu, E.A.B. Koenders, Self-healing of surface cracks in mortars with expansive additive and crystalline additive, Cem. Concr. Compos. 34 (2012) 566–574, https://doi.org/10.1016/J.CEMCONCOMP.2012.01.005.
[21] V.G. Cappellesso, T. Van Mullem, E. Gruyaert, K. Van Tittelboom, N. De Belie, Bacteria-based self-healing concrete exposed to frost salt scaling, Cem. Concr. Compos. 139 (2023), 105016, https://doi.org/10.1016/J.CEMCONCOMP.2023.105016.
[22] V. Cappellesso, D. di Summa, P. Pourhaji, N. Prabhu Kannikachalam, K. Dabral, L. Ferrara, M. Cruz Alonso, E. Camacho, E. Gruyaert, N. De Belie, A review of the efficiency of self-healing concrete technologies for durable and sustainable concrete under realistic conditions, Int. Mater. Rev. (2023) 1–48, https://doi.org/10.1080/09506608.2022.2145747.
[23] S. He, S. Zhang, M. Luković, E. Schlangen, Effects of bacteria-embedded polylactic acid (PLA) capsules on fracture properties of strain hardening cementitious composite (SHCC), Eng. Fract. Mech. 268 (2022), 108480, https://doi.org/10.1016/J.ENGFRACMECH.2022.108480.
[24] European committee for standardization, NEN-EN 197-1, Cement - Part 1: Composition, Specifications and Conformity Criteria for Common Cements, 2011.
[25] D. Snoeck, J. Dewanckele, V. Cnudde, N. De Belie, X-ray computed microtomography to study autogenous healing of cementitious materials promoted by superabsorbent polymers, Cem. Concr. Compos. 65 (2016) 83–93, https://doi.org/10.1016/J.CEMCONCOMP.2015.10.016.
[26] K.L. Scrivener, A.K. Crumbie, P. Laugesen, The interfacial transition zone (ITZ) between cement paste and aggregate in concrete, Interface Sci. 12 (4) (2004) 411–421, https://doi.org/10.1023/B:INTS.0000042339.92990.4C, 12 (2004.
[27] S. He, Z. Li, E.-H. Yang, Quantitative characterization of anisotropic properties of the interfacial transition zone (ITZ) between microfiber and cement paste, Cement Concr. Res. 122 (2019) 136–146, https://doi.org/10.1016/j.cemconres.2019.05.007.